Federica Cotugno[1], Paolo Berardino[1], Manuela Bonano[1], Antonio Ciccolella[1], Gabriella Costa[1], Felipe Martin Crespo[1], Guido Levrini[1], Michele Manunta[1], Antonio Moccia[1], Alfredo Renga[1], and Riccardo Lanari[1]

[1]Affiliation not available

May 20, 2024

Constellation Design and Analysis for Spaceborne DInSAR Mapping in Mid Inclination Orbits: the IRIDE NIMBUS Mission

Federica Cotugno, Paolo Berardino, Manuela Bonano, Antonio Ciccolella, Gabriella Costa, Felipe Martin Crespo, Guido Levrini, Michele Manunta, Antonio Moccia *Senior Member, IEEE*, Alfredo Renga, *Senior Member, IEEE*, and Riccardo Lanari*, Fellow, IEEE*

***Abstract*— The IRIDE constellation is an ambitious Italian space program that, comprising a series of small satellite sub-constellations exploiting a wide range of remote sensing technologies, will support the national authorities in their analysis and monitoring activities, with a focus on the Italian territory mapping. This paper analyses the NIMBUS X-Band Synthetic Aperture Radar (SAR) IRIDE sub-constellation, exploring potential orbital configurations beyond the more conventional and widespread Dawn-Dusk Sun-Synchronous Orbit (SSO) one. In particular, starting from the mission target, we show that a 49° Mid Inclination Orbit (MIO) in a right-looking StripMap acquisition mode represents a highly effective choice for NIMBUS, as it enhances the systematic coverage of the Italian territory with 6 days of interferometric revisit time and high spatial resolution, thereby facilitating detailed observations of both natural phenomena and anthropic activities. In addition, in terms of Differential Interferometric SAR (DInSAR) performance, we prove that MIO, besides showing no significant limitations for what attains the critical baseline and geometric distortions, allows for the recovery of the North-South deformation component that, conversely, cannot be precisely measured with DInSAR systems operating in SSO. This may lead to future advances in creating 3D deformation maps when considering the synergy between the MIO NIMBUS IRIDE satellites and SSO configurations operating with similar resolutions and wavelengths, as for the COSMO-SkyMed constellation.**

***Index Terms*— Differential Synthetic Aperture Radar Interferometry (DInSAR), constellation design, Mid Inclination Orbit (MIO), IRIDE, NIMBUS, COSMO-SkyMed.**

I. INTRODUCTION

Differential Synthetic Aperture Radar Interferometry (DInSAR) is a technique widely used in investigating ground deformations with centimeter-to-millimeter accuracy [1]-[4]. The availability of large Synthetic Aperture Radar (SAR) data archives, which started with the C-band ERS-1/2 satellites in the '90s and continued with ENVISAT in the 2000s, has encouraged the development of multi-temporal (also referred to as advanced) DInSAR techniques, capable of retrieving deformation time series, allowing us to follow the temporal evolution of the detected surface displacements [5]-[12]. The capability of the state-of-the-art DInSAR techniques to generate long deformation time series has been further enhanced by the launch of additional SAR systems operating in X-Band, such as COSMO-SkyMed (CSK), COSMO-SkyMed II Second Generation (CSG), TerraSAR-X starting from 2007, in C-Band, namely Radarsat-2 in 2007 and Sentinel-1 in 2014, and in L-Band as ALOS-2 in 2014 and SAOCOM-1 in 2018 [13]-[19]. These satellites are somehow unified by their substantial size, being all characterized by significant masses and volumes. Conversely, recent investments in SAR technology have been promoting a growing interest in constellations of small SAR satellites operating at increasing spatial resolutions (i.e., ICEYE [20] and Capella [21]) because the design, manufacturing, and feasibility of deploying several sensors through a single launch permit to cut costs compared to traditional SAR satellites. However, these systems exhibit reduced imaging capacities due to their smaller size and weight, potentially affecting the revisit time, the coverage performance, and, more generally, their DInSAR capability. Accordingly, maximizing their

This paragraph of the first footnote will contain the date on which you submitted your paper for review, which is populated by IEEE. It is IEEE style to display support information, including sponsor and financial support acknowledgment, here and not in an acknowledgment section at the end of the article. For example, “This work was supported in part by the U.S. Department of Commerce under Grant 123456.” The name of the corresponding author appears after the financial information, e.g. *(Corresponding author: Second B. Author).* Here you may also indicate if authors contributed equally or if there are co-first authors.

Federica Cotugno, Paolo Berardino, Manuela Bonano, Michele Manunta, and Riccardo Lanari are with CNR-IREA 80124, Naples, Italy (emails: cotugno.f, berardino.p, bonano.m, manunta.m, lanari.r@irea.cnr.it).

Federica Cotugno is also with the Department of Industrial Engineering, University of Naples Federico II, 80125, Naples, Italy.

Antonio Ciccolella, Gabriella Costa, and Guido Levrini are with the European Space Agency (ESA-ESRIN), 00044, Frascati, Rome, Italy (e-mails: antonio.ciccolella@esa.int, gabriella.costa@esa.int, guido.levrini@esa.int).

Felipe Martin Crespo is with Taitus Software Italia SRL, 00078, Monte Porzio Catone, Rome, Italy (e-mail:felipe.crespo@taitus.it).

Antonio Moccia and Alfredo Renga are with the Department of Industrial Engineering, University of Naples Federico II, 80125, Naples, Italy (emails antonio.moccia@unina.it, alfredo.renga@unina.it).

effectiveness may require the exploration of innovative mission configurations.

We underline that the problem of optimizing the temporal revisit of Earth Observation (EO) sensors is not brand new. Some studies used analytical methods adaptable to single satellites or symmetric constellations [21]-[24]. Other works proposed using genetic algorithms to find optimal sun-synchronous orbits (SSO) capable of covering as many target areas as possible [25]. Another recent approach [26] exploited image features of Average Revisit Time (ART) maps to design and analyze Repeat Ground Track (RGT) constellation performance, thus moving from a mathematical problem to an imaging one. Lastly, numerical methods [27]-29], consisting of dividing the Area of Interest (AoI) into grid points and analyzing their visibility from the satellite, are becoming popular too, because they are straightforward, even if time-consuming. These methods have demonstrated to be capable of maximizing the number of images for the selected AoI but cannot fully address the stringent geometric constraints imposed by the DInSAR techniques.

We also remark that most of the current remote sensing constellations exploit single plane and dawn-dusk SSOs because this simplifies the design across all subsystems, resulting in cost savings. However, in this traditional orbital design, the interferometric revisit time, namely the period between two consecutive orbital passes over the same AoI, with the same incidence angle, may easily becomes considerable and, therefore, this turns into a limiting factor due to the occurrence of decorrelation phenomena [1]. Furthermore, as DInSAR is restricted to measuring displacements along the Line-of-Sight (LOS) direction [1], the satellites in SSO can accurately measure only the Vertical and East-West displacement components projected into the radar LOS, with a clear limitation for what concerns the North-South one [30], [31]. In this context, when the focus is on mid- to low-latitude regions, Mid Inclination Orbits (MIO) may offer an effective solution to improve both the spatial coverage and the interferometric revisit time. Furthermore, an MIO DInSAR system acquires the sensibility to the North-South deformation component, thus allowing for the possible retrieval of the three-dimensional behavior of the displacement signals when properly integrated with deformation measurements derived also by SSO systems [32].

This paper focuses on the Italian constellation IRIDE, one of the most important ongoing national EO space programs, representing a next-generation constellation of small satellites. This will be completed by 2026 under the management of the European Space Agency (ESA), with the support of the Italian Space Agency (ASI), for the Italian government. We underline that IRIDE is a “constellation of constellations”, including multiple sub-constellations positioned in Low Earth Orbit (LEO), operating with mid and high-resolution capabilities. These satellites, equipped with different remote sensing technologies, comprising SAR and optical sensors, will aim to systematically map the whole Italian territory with temporally frequent data and also provide on-demand services beyond Italy. The IRIDE data will support Italian institutional entities like the Civil Protection Department and national and local Environmental Agencies in managing, preventing, and mitigating both natural and anthropogenic hazards [33], [34]. In particular, one of the SAR components of the Italian IRIDE program, called NIMBUS, is expected to include, in its first batch and design, 6 X-band small satellites deployed in Low Earth Orbit (LEO) and able to operate with various working modes and spatial resolutions [35]. Moreover, a second batch of satellites is already planned to complement the first one and to establish the complete SAR sub-constellation of the IRIDE program.

The main goal of this article is to investigate the NIMBUS orbital configuration to optimize the systematic coverage of the overall Italian territory, which is considered hereafter as our AoI, while simultaneously ensuring a short interferometric revisit time. This is achieved by introducing a simple but effective method for constellation design and DInSAR coverage analysis that considers both mission and system requirements. The orbital simulations presented in this paper have involved both SSOs and MIOs and prove that, considering the NIMBUS mission target, MIOs provide drastically better spatial coverage than SSOs with the same interferometric revisit time. Furthermore, from a DInSAR performance point of view, both the critical baseline and geometric distortions (foreshortening, layover, and shadowing) are analyzed for the chosen MIO configuration. The outcomes indicate that within the AoI the critical baseline has no significant issues, and the geometric distortions are minimal as well. However, these latter will require further consideration because the zones affected by them, remain unchanged in the Northern part of the AoI, regardless of whether the satellite is in an ascending or descending orbital pass. This is due to the slope of the MIO ground tracks that at the Northern latitudes will not significantly differ between ascending and descending cases.

The article is organized as follows. In Section II we present a brief overview of the NIMBUS mission and system requirements along with the methodology used to optimize the interferometric coverage over the AoI. In Section III we provide the necessary theoretical background for simulating and implementing the orbital behavior of satellites operating in both SSO and MIO configurations. In Section IV we apply the developed methodologies to the case study of the 6 satellites NIMBUS sub-constellation, focusing on both spatial coverage and DInSAR performance. Finally, in Section V, we present some conclusive remarks and discuss possible future developments.

II. PROBLEM STATEMENT AND METHODOLOGY

This work focuses on a SAR sub-constellation of the IRIDE program, referred to as NIMBUS, whose main parameters are detailed in Table I for the StripMap acquisition mode. Note that the considered StripMap mode is not the only available one. Indeed, the NIMBUS SAR sensors have the capability to carry out SAR imaging also through the Spotlight and Scansar modes. However, the StripMap capability is considered the baseline one for the Italian territory mapping due to its very good balance between the obtained spatial coverage capability and the achieved azimuth spatial resolution. At the current level of this satellite design, the platform is compatible with different

TABLE I
BATCH 1: PARAMETERS OF NIMBUS IRIDE SAR SUB-CONSTELLATION (STRIPMAP MODE).

Parameter	Value
Number of satellites	6
Orbital altitude range	490-550 km
Orbital inclination range	44° up to SSO
Swath width extension range	25-28 km
Access Region (off-nadir angles)	15-50°
Looking Direction	Right\Left
Radar Frequency	X band
Orbital control tube (3σ)	500 m
Max Bandwidth	215 MHz
Ground Range Resolution	2.7 m
Azimuth Resolution	2.7 m
Chirp pulse duration	50 μs
Polarization	VV

orbital configurations, namely different orbit altitudes and, more relevantly, a wide range of orbit inclinations. Accordingly, this flexibility could be exploited for orbit and constellation design in a variety of ways. Indeed, the NIMBUS satellites are theoretically compatible with single- and multi-plane constellations arranged in either sun-synchronous or lower-inclination orbits. However, the overall number of satellites for this first batch, is limited to 6 and their swath is rather narrow in size for the StripMap acquisition mode (see Table 1), which is assumed as the reference one. Moreover, two main system drivers exist in our analysis: 1) coverage of the entire Italian territory and 2) frequent interferometric revisit. With specific reference to the second driver, it is expected to make the best use of the available satellites and their pointing capabilities to minimize the time lag between two consecutive interferometric acquisitions. Based on these considerations, one can argue that a single-plane constellation is satisfactory to study and monitor localized phenomena and small-scale displacements because it ensures better geometric and temporal coherence between satellite images, thus resulting in easier data acquisition and processing. On the other hand, multi-plane constellations, despite evident advantages in terms of revisit times, are more challenging to manage, and the interferometric coverage can remain limited, due to the variability of the observation geometry. As a trade-off solution to optimize temporal and spatial coverage without increasing system complexity, MIOs can be used, notably for latitudes close but lower than the orbital inclination, where the orbital ground tracks are much more tilted, and the inter-track distance is, therefore, increasingly reduced. In the context of interferometric applications, it is essential to think in terms of RGT orbit, namely an orbit that retraces its R ground tracks after N nodal days, that is the time the Earth needs to complete an overall rotation with respect to the line of nodes (i.e., a straight line joining the intersections between the orbit plane of the satellite and the orbit plane of the Earth). In this paper, our focus is on configurations where, being N_{Sat} the number of satellites,

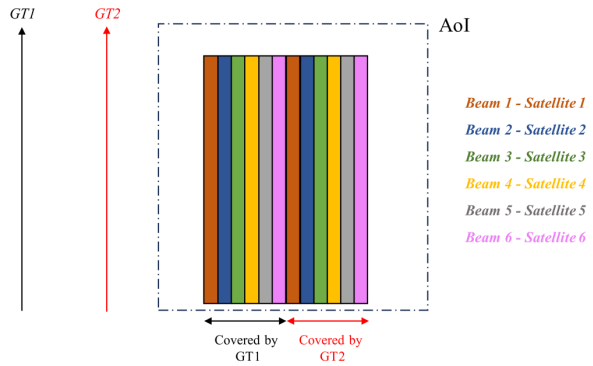

Fig. 1. Coverage strategy between two consecutive Ground Tracks (GT).

$\frac{N}{N_{Sat}}$ is an integer number, which is a widely used configuration in single-plane constellations.
This enables both fast revisit and repetitive geometry because the complete pattern of the R tracks, that one satellite would fulfill in N nodal days, is completed in $\frac{N}{N_{Sat}}$ days by the constellation. Indeed, different satellites share the same nominal ground track for this type of constellation. Once the orbital configuration of the constellation is set, the interferometric coverage strategy over the AoI, is the following one. Specifically, to fill the gap between two consecutive ground tracks in the shortest possible time by using the onboard payload's swath width, each SAR satellite in the constellation is assigned a distinct beam for the entire orbital cycle of N nodal days. This means that the first satellite uses only the first beam, the second satellite only the second, and so far, until all beams are employed. In such a way, when the satellite passes again at time t_N (after N nodal days) on the same RGT over which it transited at time t_0, it re-observes the same area with the same angle of incidence used at t_0. A sketch of this strategy is represented in Fig. 1, where 6 different beams, corresponding to the same average swath width and assigned to 6 different satellites, are needed to fill the gap between the ground tracks. With this methodology, the N nodal days are the time required for the constellation to complete the interferometric coverage since the acquisitions made at t_0 and t_N are interferometrically compatible with each other for a given target area.

III. CONSTELLATION DESIGN AND COVERAGE ANALYSIS

The RGT orbits are necessary for DInSAR applications [1]. For this reason, iterative algorithms have been implemented in this work to obtain RGT in the case of both SSOs and MIOs. Atmospheric drag, solar radiation pressure and high-order gravitational harmonics are not used for orbit design, because, as for standard practices, suitable orbital maintenance maneuvers are assumed to counteract these effects. Accordingly, following this RGT orbit design, a simulation tool of spatial and temporal coverage capabilities, that implements the strategy discussed in Section II, is carried out to validate the chosen satellite configuration.

A. RGT Orbit Design

The condition of repeating ground-track orbit does not change from high to mid-inclination orbits. Specifically, the repetition factor Q, which represents the number of orbits completed per day, can be calculated as [36]:

$$Q = \frac{\dot{M}(\alpha, i, e) + \dot{\omega}(\alpha, i, e)}{\Omega_{\oplus} - \dot{\Omega}} \quad (1)$$

where α is the orbit semimajor axis, i is the orbital inclination, e is the orbit eccentricity, $\Omega_{\oplus}$ is the angular rate of the Earth rotation expressed in the Earth Centered Inertial (ECI) reference frame, $\dot{M}$ is the mean motion (velocity) of the satellite, $\dot{\Omega}$ is the precession rate of the line of nodes, $\dot{\omega}$ is the precession rate of the line of apsides. These latter parameters exhibit a secular variation due to the Earth's oblateness second gravity coefficient J_2, which can be modeled as [37]:

$$\begin{aligned} \dot{M} &= \sqrt{\frac{\mu}{\alpha^3}}\left[1 + \frac{3}{2} J_2 \frac{\rho_{eq}}{\alpha(1-e^2)}\sqrt{1-e^2}\left(1 - \frac{3}{2}(\sin i)^2\right)\right] \\ \dot{\omega} &= \frac{3}{2} J_2 \left(\frac{\rho_{eq}}{\alpha(1-e^2)}\right)^2 \left(2 - \frac{5}{2}(\sin i)^2\right) \\ \dot{\Omega} &= -\frac{3}{2} J_2 \dot{M} \left(\frac{\rho_{eq}}{\alpha(1-e^2)}\right)^2 \cos i \end{aligned} \quad (2)$$

where μ is the gravitational constant of the Earth and ρ_{eq} is the mean equatorial radius of the Earth. Adopted values for the parameters of interest are listed in Table II.

TABLE II
ADOPTED VALUES [38].

Parameter	Value
$\Omega_{\oplus}$	7.2921 x 10^{-5} rad/s
J_2	0.0010826
μ	3.9860 x 10^5 km^3/s^2
ρ_{eq}	6.3781 x 10^3 km

According to (2), the line of nodes precession is negative for the MIO case, occurring in the opposite direction than the Sun rotation. Thus, both Sun rotation and Right Ascension of the Ascending Node (RAAN) precession contribute to the changing Local Time of the Ascending Node (LTAN). The drift of LTAN as a function of satellite altitude and for different values of the orbit inclination is shown in Fig. 2. This variety will cause the satellite to revisit the same area but at different local times. Although this latter turns out to be something to consider when processing data due to the different effects the atmosphere would have on the radar acquisition, a nontraumatic impact on the results is expected. Hence, altitude, inclination and eccentricity can be adjusted to match the following condition [36]:

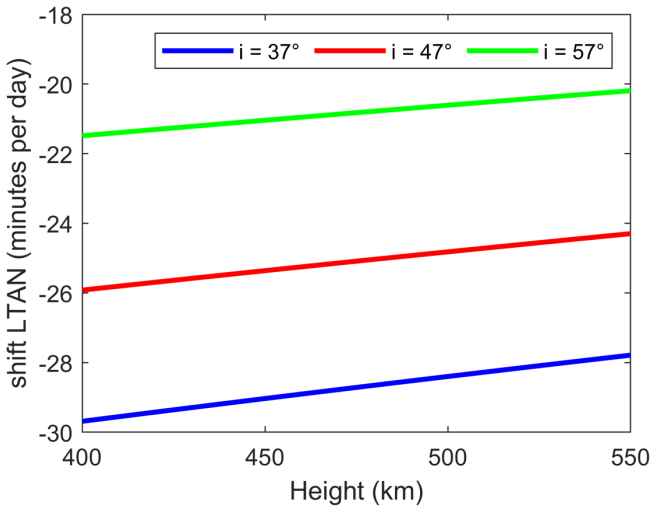

Fig. 2. Drift of LTAN for three different MIOs.

$$Q = \frac{R}{N} \qquad R, N \in \mathbb{N} \quad (3)$$

being R the number of ground tracks completed in N nodal days. Considering for the sake of simplicity the case of circular orbits, and setting the inclination to a specific, input value, the height of the satellite is the only free parameter to adjust to realize repeated passes over the same area after N nodal days. Assuming an initial attempt value of the height that is compliant with our mission, a preliminary estimate for the repetition factor Q can be computed by considering (1). The integer part of this value is exploited to define a range of potential values for R, as follows:

$$[(int(Q) - 1) * N, (int(Q) + 1) * N] \quad (4)$$

where int indicates the operator for extracting the integer part. The value of R that, substituted in (3), corresponds to a height closest to the initial attempt value is then selected. To verify the outcome, Wagner's algorithm [39] can be also used. This is an iterative numerical method that takes R, N, and the orbital inclination as input and calculates the value of the semi-major axis. Accordingly, this latter algorithm only considers the second zonal harmonic J_2 effect.

B. RGT Orbits Propagation

An orbit propagator has been implemented in order to support the constellation design and preliminary coverage analysis. From the value of the semimajor axis and inclination, the orbits have been propagated to obtain RGTs in the ideal condition of a null orbital tube, as the satellite returns perfectly to its previous trajectory. Although the propagator uses the approximation of spherical Earth for coverage analysis and circular orbits, it still considers the secular effect of J_2. Within the proposed propagation algorithm implementation, the first parameter that is introduced is the angular velocity $\dot{u}$ of the satellite with respect to the ascending node, calculated as the

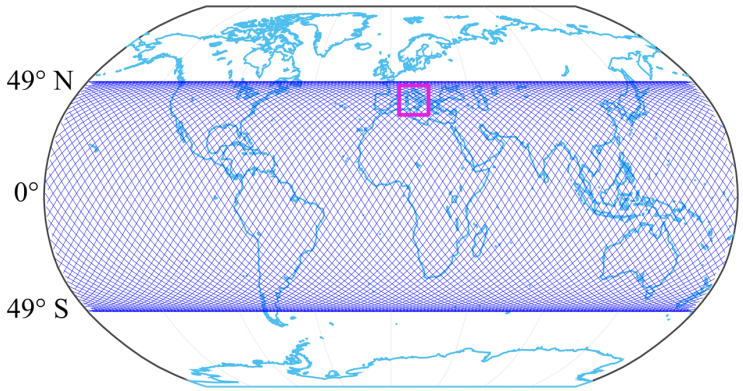

Fig. 3. RGT of a satellite with R=89, N=6, and an orbital inclination angle of 49°. The box highlights Italy which corresponds to the AoI of the IRIDE NIMBUS mission.

sum of the mean motion and the precession velocity of the line of axes [37]:

$$\dot{u} = \dot{M} + \dot{\omega} \tag{5}$$

Based on the value of $\dot{u}$, we can compute the orbital nodal period, say τ_N , that is the time to fly from the ascending node to the consecutive one [37]:

$$\tau_N = \frac{2\pi}{\dot{u}} \tag{6}$$

Once the nodal period is known, it is possible to determine the shape of the satellite ground track in terms of latitude and longitude, with an assigned sampling step, say 1 second. The latitude Φ_s is obtained by the only contribution of the motion of the satellite, as follows [37]:

$$\sin \Phi_s = \sin u \sin i \tag{7}$$

where u, referred to as the argument of latitude, is the angle in the orbit plane from the ascending node to the satellite position. The longitude λ is achieved through the following sum [37]:

$$\lambda(t) = \lambda_{AN}(0) + \lambda_s(t) - (\Omega_\oplus - \dot{\Omega})t \tag{8}$$

where $\lambda_{AN}(0)$ is the initialization of the longitude of the ascending node, $(\Omega_\oplus - \dot{\Omega})t$ is the contribution of the rotation of the Earth to be subtracted, $\lambda_s(t)$ is due to the motion of the satellite, this latter given by [37]:

$$\tan \lambda_s = \tan u \cos i \tag{9}$$

In concluding this section, it is important to point out that this simplified algorithm is implemented as a quick tool to obtain a first-order estimate of the coverage and revisit time. More complex tools and software for orbit propagation and coverage analysis could be also used (see Section IV).

C. Orbits Apparent Inclination

Fig. 3 shows an example of an RGT orbit obtained as the output of the implemented propagator. In detail, an MIO with an orbital inclination of 49°, for the case of 89 revolutions completed in 6 nodal days is depicted. From Fig. 4, it is evident that the ground tracks tend to exhibit a near-horizontal orientation at latitudes close to the orbital inclination angle. This effect can be represented by the apparent inclination ϑ_s or slope of the orbital ground track with respect to the parallel at an assigned latitude, which can be computed as [36]:

$$\tan\vartheta_s = \frac{\sqrt{(\sin i)^2 - (\sin\varphi)^2}}{\cos i - \frac{(\cos\varphi)^2}{Q}} \tag{10}$$

where φ is the latitude of interest, i is the orbital inclination and Q is the repetition factor of the orbit [37]. The inter-track distance SW_φ, i.e., the distance between two adjacent ground tracks, can be computed, at a first approximation, as follows [36]:

$$SW_\varphi \approx \frac{2\pi\rho_{eq}\cos\varphi \sin\vartheta_s}{R} \tag{11}$$

By analyzing (11), we can infer that the inter-track distance changes with the latitude φ, and it is the smallest at latitudes close to the orbital inclination angle and the largest at the equator.

A useful constraint to consider is the link between the number of satellites, the swath width of the payload (i.e., the SAR system), and the inter-track distance at the Southernmost latitude of the AoI, which represents the maximum possible distance at which orbital ground tracks can occur within the assigned AoI. Based on this, once the number of satellites of the constellation is known, the payload's swath width of each satellite, required for satisfactory coverage over the AoI, can be estimated as follows:

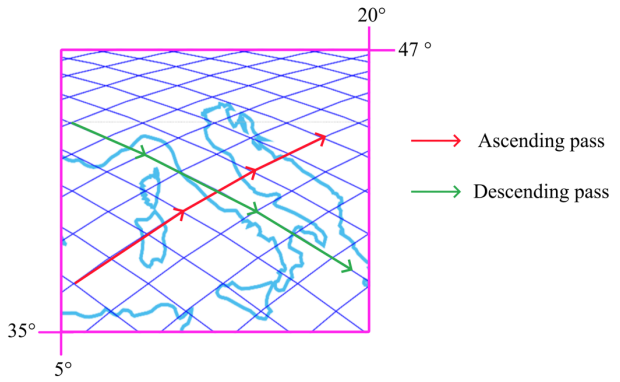

Fig. 4. Detailed zoom - in view over Italy (AoI). Two examples of ascending and descending passes of the 49° MIO configuration are highlighted by red and green colors, respectively.

$$SW_{payload} = \frac{SW_{southernmost\ place\ of\ the\ AOI}}{number\ of\ satellites} \quad (12)$$

Although for the case study herein discussed there is no need to compute the payload swath width as it is known (see Table I), (11) and (12) still provide a first attempt estimate which is helpful in assessing the eligibility of an orbital configuration during an EO mission design process.

D. Revisit Time and Coverage Analysis

The constellation design cannot rely on orbit propagation only and a tool for coverage analysis must also be used. The first step involves establishing a grid of points over the AoI. To assess the visibility of a ground point from the satellite, we first compute the values of the sensor-point distance, as the satellite progresses along its orbit, and we select the azimuth position in correspondence with the minimum distance value (zero-doppler position). To establish if the target falls into the satellite swath, we check whether its off-nadir angle is within the satellite beam. In light of the aforementioned, it is necessary to assign a beam to each satellite in order to have a representation of the spatial extent of a satellite's observation, namely the swath width of the SAR system onboard. Since the NIMBUS satellite beams have not yet been assessed, it is possible to hypothesize them through merely geometric considerations. Indeed, with reference to Fig. 5, the height of the satellite and the sensor average swath width are known parameters. For the first beam (first satellite), a value of the near-range off-nadir angle δ_1 is set, ensuring in this way the retrieval of the far-range off-nadir angle δ_2. Then, the operation is reiterated by considering δ_2 as the starting near-range off-nadir angle of the subsequent beam. Thus, the final output consists of a series of beams, each corresponding to the number of satellites, without any overlap among them, as the end of one beam aligns precisely with the start of the immediately succeeding one. However, it is essential to specify that the presented beams are geometrically designed to facilitate coverage analysis since the actual beams of a real SAR system, instead, typically exhibit a mutual overlap. As a final point, the simulator is completed with the capability to consider SAR satellites working in either left- or right-looking mode. This is implemented by introducing a control on

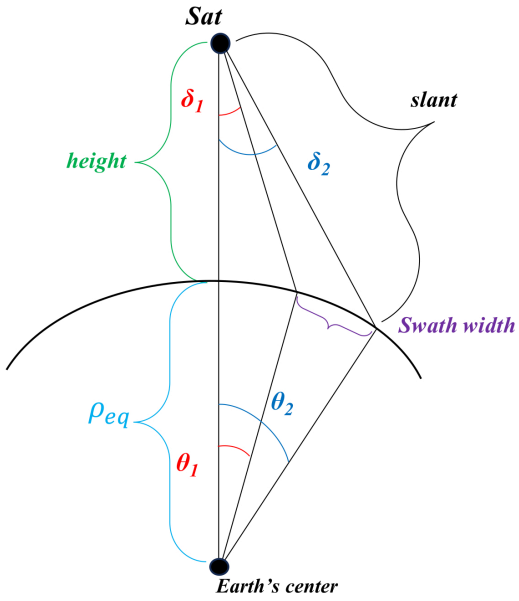

Fig. 5. Observation Geometry.

longitudes. The logic, depicted in Fig. 6, is as follows: if one supposes that the satellites operate in right-looking mode and a target point is set on the ground:

1) when observing from an ascending pass, if the position of the orbiting satellite is at a lower longitude than that of the location of the point target, it indicates that the target is positioned to the right of the satellite, therefore, it is an observably feasible one.
2) when observing from a descending pass, if the position of the orbiting satellite is at a greater longitude than that of the location of the point target, it indicates that the target is positioned to the right of the satellite, therefore, it is an observably feasible one.

IV. THE IRIDE NIMBUS MISSION

The above-described tool in Section III is designed to receive RGTs of different types as input, including both SSOs and MIOs. Accordingly, by using the developed tool, it is possible to compare the interferometric performance of the RGT orbits both in terms of revisit time and coverage of the AoI. Concerning the IRIDE program and, in particular, the NIMBUS SAR sub-constellation, a test is performed using a single-plane configuration composed of 6 satellites, thus acquiring data over the Italian territory with 6 beams, with an average swath width of 27.5 km. Since, as previously stated in Section II, this work examines orbits wherein the number of days for orbital cycle repetition is either identical or a multiple of the number of satellites within the constellation, it is worthwhile to evaluate the performance of a 6-satellite constellation where the orbital cycle lasts, nominally, only 6 nodal days. This is in line with the EO community increasing interest in reducing the revisit time, which is beneficial for monitoring the target areas, particularly in the DInSAR framework. Valuable choices have

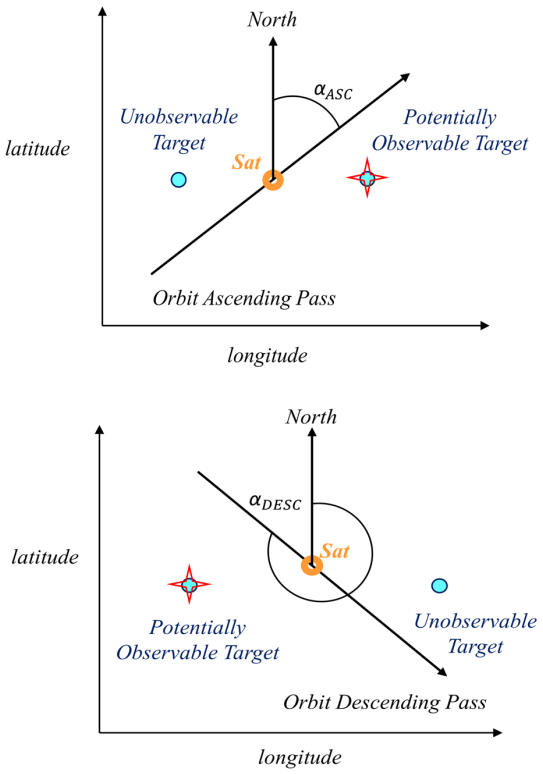

Fig. 6. Sketch of the implemented right-looking acquisition mode logic for ascending and descending MIO passes. The logic does not change in the right-looking mode SSO case.

been identified within both MIO and SSO, taking into account these premises, as well as the specifications of the IRIDE NIMBUS system. The selected orbital inclination value in the case of MIO is the outcome of several geographic and SAR system considerations. First of all, we remark that Italy extends up to a maximum latitude of about 47.5°N. In addition, as the SAR systems operate in side-looking mode, they require off-nadir angles that are large enough not to compromise their imaging capabilities because of geometric and radiometric distortions. In particular, we can assume that off-nadir angles must be greater than 20°. Furthermore, by analyzing (10) and (11), it is clear that, for an assigned latitude φ, the inter-track distance SW_{φ} increases with increasing orbital inclination angle i. Accordingly, if the i value is too high, some parts of the Southern AoI could remain unobserved, as clearly shown in the following Section IV-A.

On the other hand, selecting orbital inclination angles below the maximum AoI latitude (e.g., 47.5°N for Italy), reduces the potentially observable areas outside the AoI (Fig. 3). Indeed, though this constellation aims for systematic coverage of the Italian territory, it should also serve for on-demand acquisitions outside Italy, when requested. It is worth noting that when the orbital inclination angle is smaller than the maximum AoI latitude, the full Italian territory mapping can be reached only with the left-looking acquisition mode, in order to guarantee the coverage of the Northernmost regions (Fig. 4).

Based on these considerations, the orbital inclination angle that does not present an excessive inter-track distance in the AoI Southern part, thus guaranteeing the full coverage of the target area, results to be 49°. Indeed, this value allows for observations of Northern Italy at off-nadir angles great enough (i.e., we can assume 20° as a reference) and maximizes on-demand targeted observations beyond the AoI. Finally, it is clear that at a 49° orbital inclination, the most efficient observation mode for our AoI is the right-looking one, with whom we can achieve almost full coverage in Central-Southern Italy and take advantage of many close orbital passes in the Northern region, as clearly shown in the detailed coverage analysis presented in the following Section IV-A.

Table III summarizes the orbital characteristics of both the chosen MIO configuration and the SSO 6-day RGTs.

TABLE III
ORBITAL PARAMETERS OF THE IRIDE NIMBUS SEED SATELLITE IN BOTH SSO AND MIO CASES.

Orbital Parameter	SSO	MIO
Height	509.95 km	548.18 km
Inclination	97.44°	49°
Eccentricity	0	0
Number of revolutions	91	89
Revisit time (Nodal days)	6	6

A. Spatial Coverage Analysis

First, a rectangular grid is considered over the Italian territory with points sampled at 0.25° intervals in both latitude and longitude directions. The grid encompasses latitudinal coordinates between 36.5° and 47.5° and longitudinal coordinates between 6.5° and 19.0°. The coverage of the national territory in both the SSO and MIO cases, achieved with the beam configurations listed in Table IV, is thus visually represented in Figs. 7(a)-(d). Orbital passes are depicted in red, while colored dot points with the cross symbol represent the areas illuminated by the SAR sensor.

TABLE IV
BEAMS ASSIGNMENT WITH A 27.50 KM SWATH.

Satellites	Beams (Off Nadir Angle, SSO case)	Beams (Off Nadir Angle, MIO case)
Satellite 1	22.00° - 24.55°	22.00° - 24.37°
Satellite 2	24.55° - 26.98°	24.37° - 26.64°
Satellite 3	26.98° - 29.30°	26.64° - 28.81°
Satellite 4	29.30° - 31.49°	28.81° - 30-88°
Satellite 5	31.49° - 33.58°	30.88° - 32.84°
Satellite 6	33.58° - 35.55°	32.84° - 34.71°

It is evident that the 49° MIO right-looking case achieves almost complete coverage in 6 nodal days, whereas the same result is impossible to reach through the SSO one with the same parameter. More specifically, an SSO constellation can map the AoI only in a longer time frame, i.e., $N = 12$ or 18 nodal days. On the other hand, we remark that MIO orbits represent the highly effective choice when the mission requires the systematic coverage of a specific AoI at mid-latitudes, as in the

IRIDE NIMBUS case. However, we also underline that if the mission objective were to achieve global coverage, then SSOs would be the only viable option because their ground tracks span the entire globe.

For the sake of completeness, it is also important to point out that even for the considered MIO there are still some areas in the South of the AoI, which are slightly outside the covered swath. This is attributed to the increasing separation between consecutive orbital tracks as we move closer to the equator (see (11)). Accordingly, a wider acquisition swath would be needed to cover the expanding intervals. Indeed, based on (11) and (12), the inter-track distance at the Southernmost point in Sicily (36.64°N 15.08°E) is ~217.50 km, that implies for each satellite a required average swath width of about 36.25 km. However, this does not pose a concern since a second NIMBUS batch that will work cooperatively and complementarily with the first one will likely be launched in the future. Moreover, these coverage holes could be partly mitigated by exploiting the chirp "tails", which are the regions in the near- and far-range fields of the SAR image where the spatial resolution undergoes a limited degradation. Figs. 8(a) and (b) show the detail of these critical zones to visualize the unobserved points, where a grid denser than the one used in Fig. 7 is applied, i.e., the points are spaced 0.10° apart in both latitude and longitude.

To corroborate the results of the developed coverage tool, a further validation step has been carried out by exploiting the

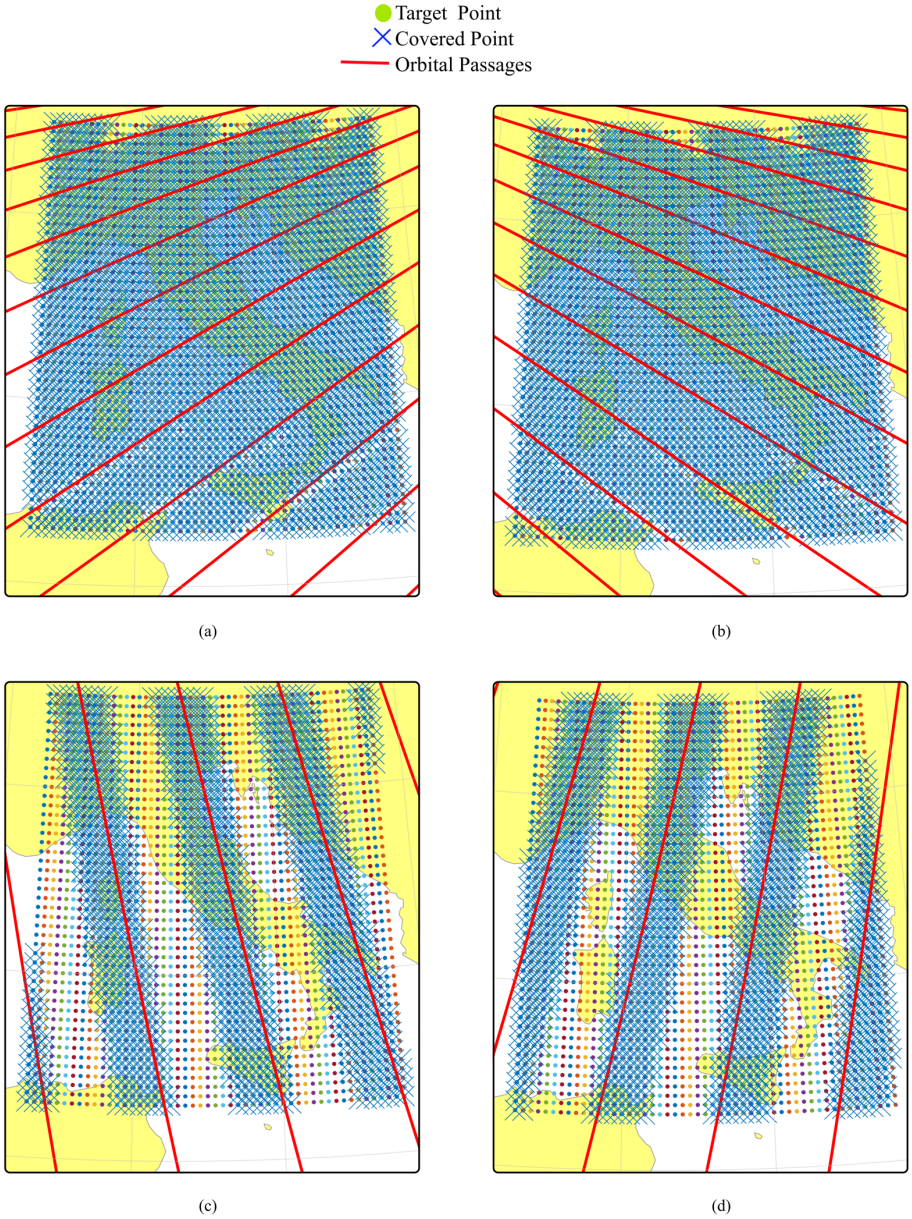

Fig. 7. Coverage simulation over the Italian territory achieved by a constellation of 6 satellites each acquiring with a 27.5 km swath width and a right-looking acquisition mode. Colored points represent the targets, whereas the crosses point to the covered (illuminated) areas. (Top) 89 MIO passes in 6 days for (a) ascending case and (b) descending case. (Bottom) 91 SSO passes in 6 days for (c) ascending case and (d) descending case.

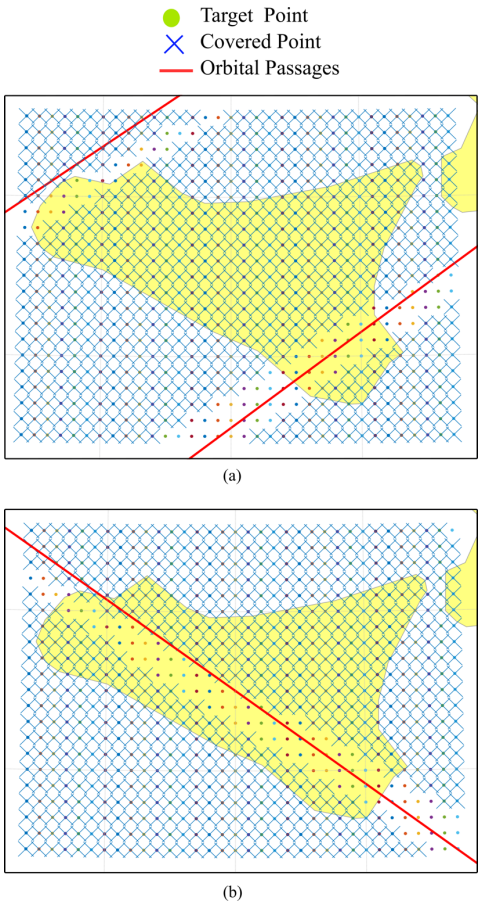

Fig. 8. Detail of coverage analysis on Sicily (South region of the AoI) with a 27.5 km swath width. Colored points represent the targets, whereas the crosses point to the covered (illuminated) areas. 89 MIO passes in 6 days. Right-looking acquisition mode (a) ascending case (b) descending case.

SaVoir software [40]. The outcome of this additional experimental test is illustrated in Figs. 9(a) and (b). The agreement between the results in Figs. 7 and 9 is evident, thus confirming the validity of the implemented tool.

In complementing the results related to the coverage of the Italian territory with a 49° MIO, further considerations have been made regarding the duty cycle. By leveraging the initial and final time of each observation, it is feasible to estimate the acquisition time of any orbital pass over the AoI, as depicted by the histogram in Fig. 10, reporting the 30 orbital passes over Italy. Additionally, Fig. 10 illustrates the corresponding behavior of the duty cycle, obtained as the ratio between the acquisition time and the orbital period of the satellite; this latter is computed by using (6) and amounting to 5731 seconds. It is worth noting that such acquisition times have been calculated over the whole AoI, including both sea and land coverage. This histogram reveals an average acquisition time of 141 seconds, corresponding to an average duty cycle of 2.47%. This is another very interesting outcome because it shows that it is possible to effectively map the Italian territory within 6 days using reduced duty cycles compared to those much larger needed for SSO orbits (around 600 seconds to cover the Italian territory).

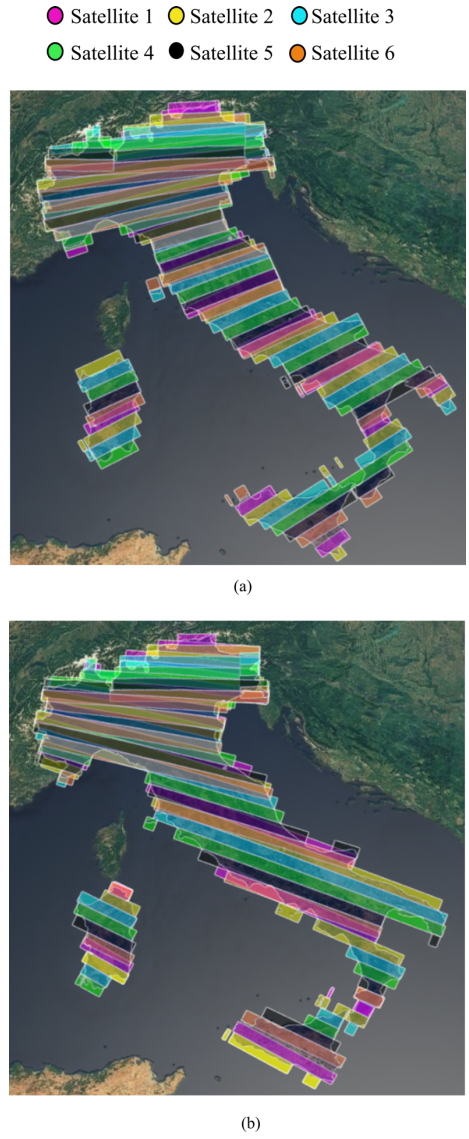

Fig. 9. Coverage simulation over the Italian Territory (SaVoir) achieved by a constellation of 6 satellites each acquiring with a 27.5 km swath width and a right-looking acquisition mode. 89 MIO passes in 6 days (a) ascending case (b) descending case.

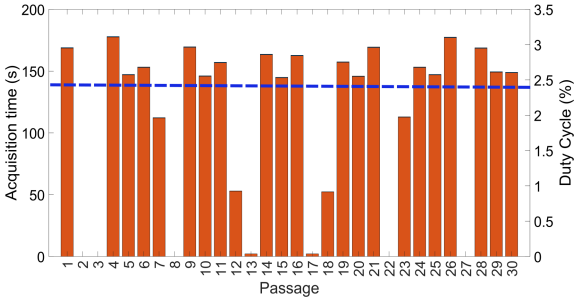

Fig. 10. Acquisition time and duty cycle of each 49° MIO passage over Italy. The blue dashed line highlights the average values of acquisition time and duty cycle.

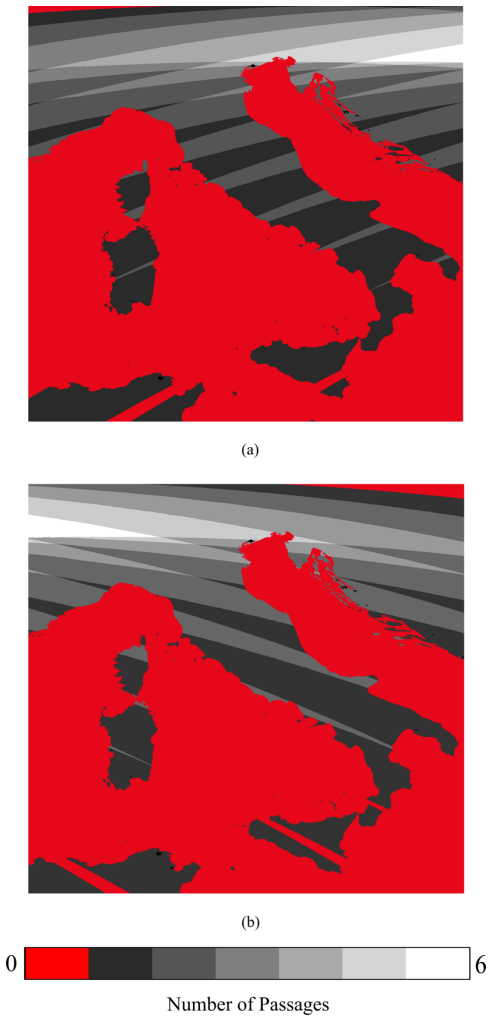

Fig. 11. Number of orbital passes for 49° MIO, right-looking acquisition mode (a) ascending and (b) descending cases.

B. Interferometric Performance

Once the spatial coverage analysis is assessed, it is worth analyzing whether the result obtained over the Italian territory with a 49° inclination and 6-day repetition orbit exhibits interferometric performance that successfully supports the DInSAR exploitation of this MIO configuration. To account for local topography effects, the SRTM Digital Elevation Model (DEM) sampled at 3 arcsec is used. Hence, the first parameter that is analyzed is the critical perpendicular baseline, defined as follows [41]:

$$l_{\perp} = \frac{\lambda \cdot r \cdot tan(\gamma)}{2\Delta r \cdot cos(\delta - \beta)} \tag{13}$$

where λ is the wavelength, Δr is the slant range resolution, β is the angle between the horizontal direction and the vector connecting the center of the orbital tube with the satellite position, r is the sensor-target range distance, δ is the off-nadir angle, set equal to those presented in Table IV in the 49° MIO case, and γ is the local incidence angle, i.e., the angle between the satellite LOS and the local normal to the facet of the DEM. We remark that in the NIMBUS case, λ is set equal to 0.031 m, Δr is assumed to be 2 m and β is set equal to $\frac{\pi}{4}$, this latter identified so as not to overestimate the critical baseline and obtain plausible values. Based on these assumptions, critical perpendicular baseline maps have been generated for both MIO ascending and descending passes over Italy. We remark that because of orbital inclination, as explained in Section III, in the Southern part of the AoI, the orbital passes are sparser and some gaps in coverage occur. Conversely, as we move Northward, the number of passes over the same area increases; thus, at the same DEM point, multiple perpendicular critical baseline values are possible. The discrepancy between the number of passes occurring in the South and North of the AoI is illustrated in Figs. 11(a) and (b). Therefore, maps representing both maximum (best case) and minimum (worst case) critical perpendicular baseline values are generated. It is straightforward to note that if only one orbital pass occurs at a DEM point, there exists solely one possible value of critical perpendicular baseline. From the maps depicted in Figs. 12 (a)-(d), it emerges that most of the DEM points exhibit a critical perpendicular baseline larger than 500 m. Specific percentages are listed in Table V. However, to carry out a full assessment we also show in Table V the percentage of DEM points exhibiting a critical perpendicular baseline larger than 1500 m (i.e., three times the IRIDE NIMBUS orbital tube). Note that the obtained perpendicular critical baseline values are large enough to conclude that the 49° MIO configuration does not pose a significant issue for what concerns this parameter.

TABLE V
PERCENTAGE OF DEM POINTS HAVING A PERPENDICULAR CRITICAL BASELINE GREATER THAN 500 M AND 1500 M.

	MIO Ascending Case	**MIO Descending Case**
Points with a Minimum Critical Perpendicular Baseline ≥ 500 m	95 %	92 %
Points with a Maximum Critical Perpendicular Baseline ≥ 500 m	95 %	93 %
Points with a Minimum Critical Perpendicular Baseline ≥ 1500 m	80 %	77 %
Points with a Maximum Critical Perpendicular Baseline ≥ 1500 m	87 %	84 %

Further aspects that could jeopardize the SAR imaging, capabilities of the system, and thus also the DInSAR applications, are the geometric distortions, i.e., the foreshortening, layover, and shadow effects [1]. To quantify them, we set thresholds on the values of the local incidence angles. These thresholds are retrieved by exploiting the *R-index equation* [42]:

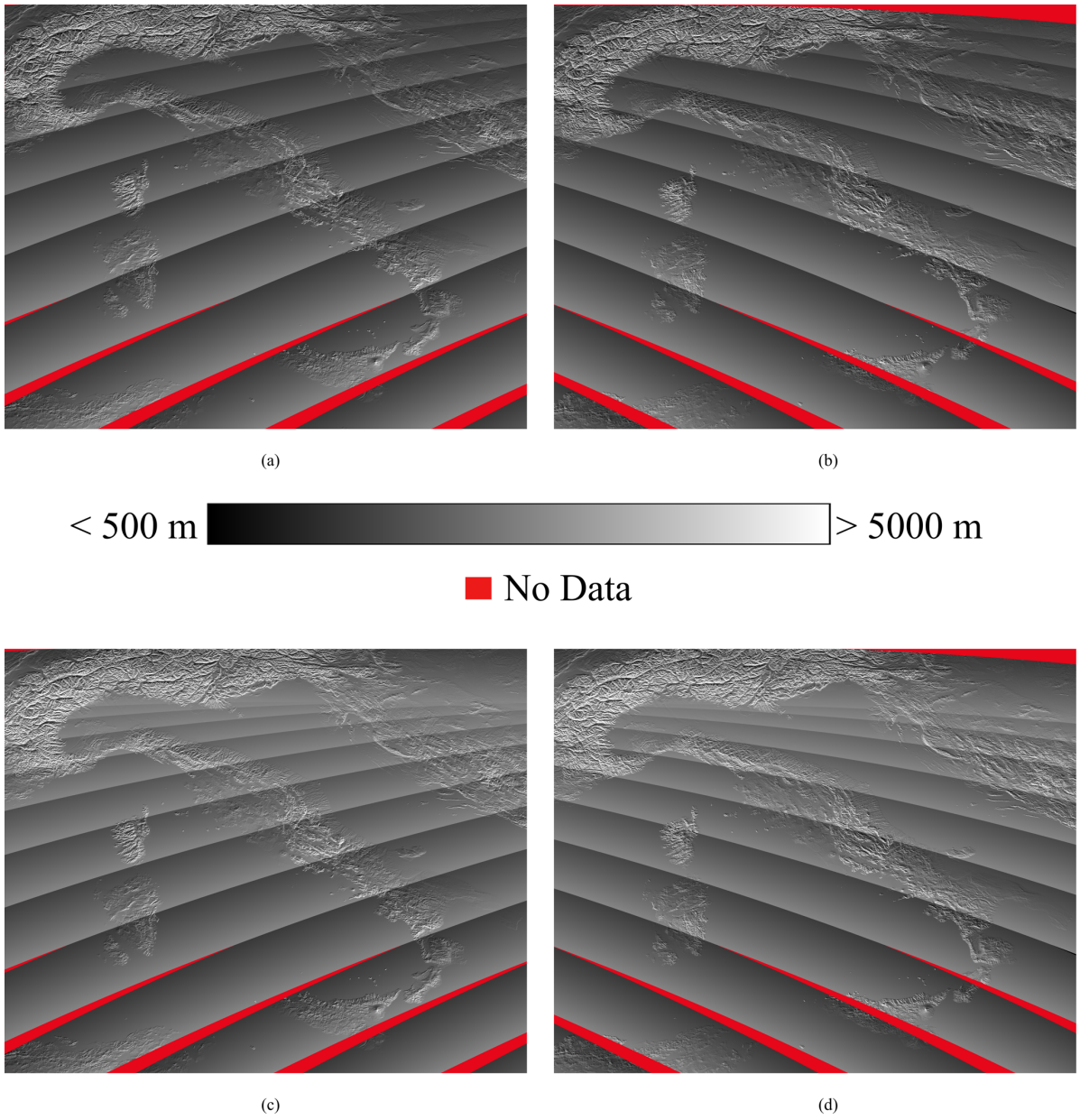

Fig. 12. (Top) Minimum perpendicular critical baseline maps in a 49° MIO, right-looking acquisition mode for (a) ascending case and (b) descending case. (Bottom) Maximum perpendicular critical baseline maps in a 49° MIO, right-looking acquisition mode for (c) ascending case and (d) descending case. Red areas are related to gaps in coverage (no data).

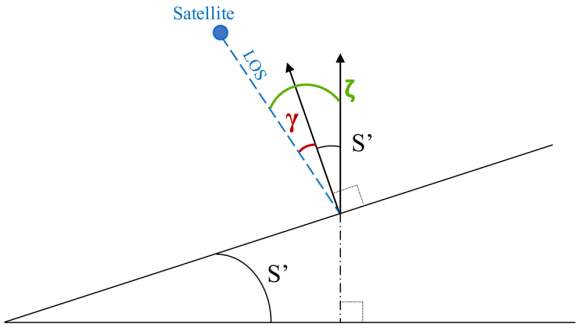

Fig. 13. *R-index* equation parameters, see (14).

$$R_{index} = -sin(S' - \zeta) = \sin(\gamma) \quad (14)$$

where S' is the slope derived from DEM and computed in the plane perpendicular to the satellite flight path, while ζ and γ represent the incidence angle computed with respect to the Vertical and the local normal directions, respectively. For the sake of clarity, these quantities are illustrated in Fig. 13.
Assuming a *R-index* value of 0.25, corresponding to an *R-index* class with high pixel compression due to the negative impact of the slope [42], we can easily achieve that the foreshortening and layover effects occur at local incidence angles γ in the interval [-15°,15°]. Regarding the shadow effect, which nominally occurs when the local incidence angle is greater than 90°, it is

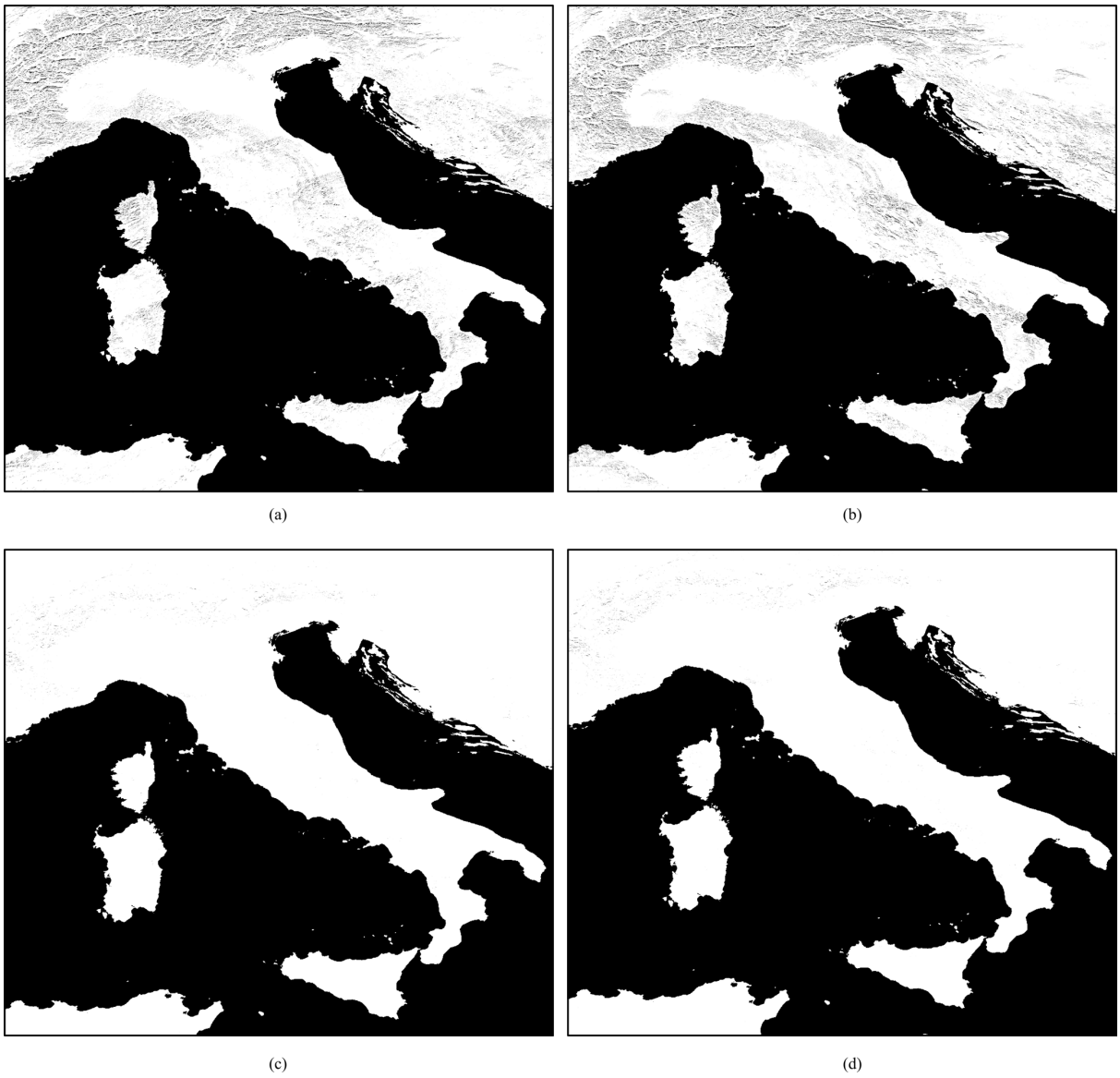

Fig. 14. Masks of geometric distortions in a 49° MIO, right-looking acquisition mode. Black areas are affected by the phenomena of geometric distortion and thus do not appear to be in the SAR visibility. (Top) Foreshortening/Layover mask for (a) ascending case and (b) descending case. (Bottom) Shadow mask for (c) ascending case and (d) descending case.

assumed to arise when the local incidence angle is greater than 75° (i.e., 90° − 15°, consistent with the 15° chosen for foreshortening/layover thresholds). The foreshortening/layover and shadow masks are depicted in Figs. 14(a)-(d). In both the ascending and descending cases, only 4% of the DEM points are negatively impacted by foreshortening/layover effects, mainly in mountainous areas, as expected. This confirms that the applicability of MIO is not significantly affected by these geometric distortions. Moreover, the smallness of these phenomena is consistent with the above-discussed results of the critical perpendicular baseline, which, as noted, is generally high enough over the AoI. Indeed, foreshortening and layover effects, arising at small local incidence angles, result in low critical perpendicular baseline values, as inferred from (13). Moreover, the shadow has an even lower impacting effect, i.e., about 0.1 % of the DEM points, as shown in Figs. 14(c)-(d). It is worth noting that these geometric distortions tend to coincide in the Northern regions due to the nearly horizontal (East-West) slope of the orbits, which always illuminates the same areas, regardless of whether the orbital pass is ascending or descending.

In Figs. 15(a)-(b) a detailed zoom-in view of the foreshortening/layover in Northern Italy is depicted, while in Fig. 15(c) the common map of these effects has been created, showing that 70% of the points in foreshortening/layover are common to both the ascending and descending cases. This offers some interesting insights into the design of the second batch of NIMBUS, which is already planned. In this regard, if we choose for this second batch an MIO with a left-looking acquisition mode, and a different orbital inclination angle, we can free these Northern Italian regions from the foreshortening/layover problem, since such geometric

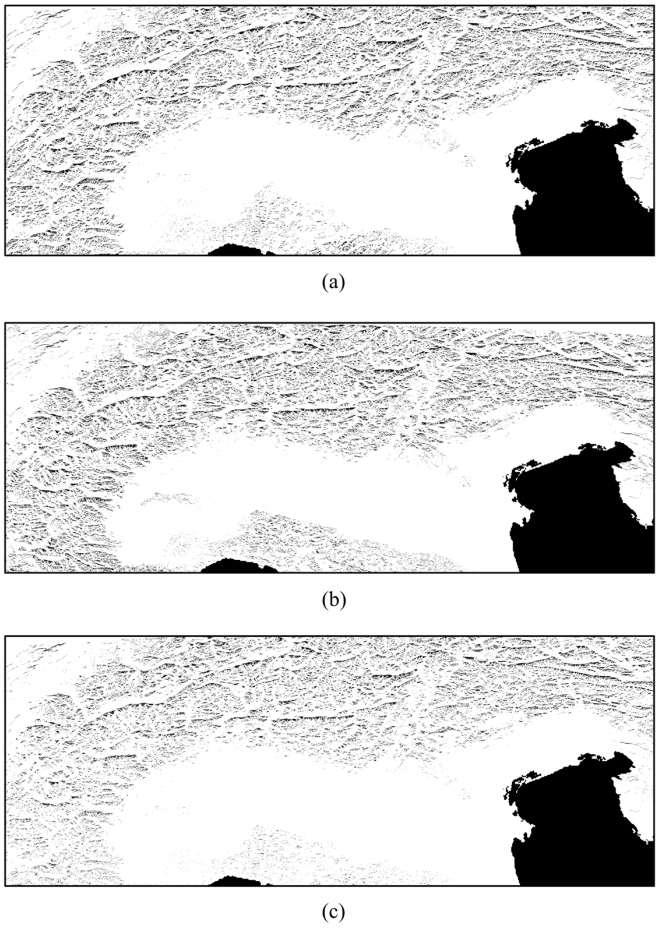

Fig. 15. Detailed zoom-in view of foreshortening/layover effects over Northern Italy. (a) MIO ascending passes (b) MIO descending passes (c) common map (ascending and descending passes). The observable zones (corresponding to the white areas) and the zones affected by foreshortening/layover phenomena (black ones) are almost coincident.

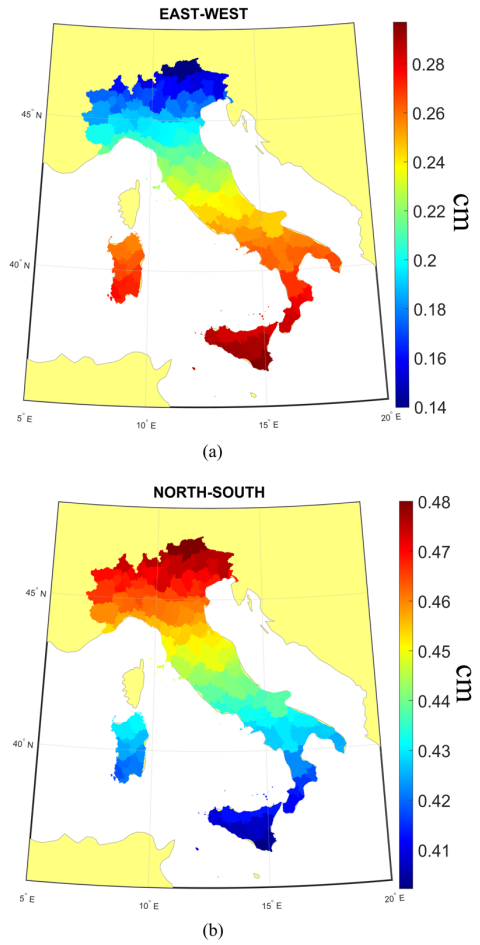

Fig. 16. Simulation map showing the projection along the LOS in correspondence to 1 cm deformation (a) in the East-West direction (b) in the North-South direction.

distortion phenomena would occur on the opposite mountain slopes, reversely to the situation of the first batch.

As introduced in Section I, another key advantage of MIO configurations is the capability of overcoming the issue related to the very poor sensitivity toward the North-South deformation component of the SSO one. Indeed, the challenge is to have IRIDE NIMBUS, arranged in an MIO configuration, working synergistically with an SSO constellation operating at a similar wavelength (X-band) and comparable resolution (2-3 meters), such as the CSK/CSG one, which has been mapping the whole Italian territory through the Map Italy program [43]. Thus, from the combined work of these two constellations, being able to measure all three displacement components (i.e., Vertical, East-West, North-South), we can finally retrieve 3D deformation measurements with unprecedented accuracy and pixel density. Having ascertained that the cooperation with SSO constellations as for the CSK/CSG case may allow for the retrieval of the 3D deformation field, our focus now narrows to the independent functionalities and inherent limitations, within the context of deformation equations, of only the first batch of the NIMBUS IRIDE constellation arranged in a 49° MIO. To quantify the impact of the proposed configuration in estimating the North-South displacements, we can use the typical LOS projection formulas [44]:

$$\begin{aligned} d_{losAsc} &= d_{up}\cos\delta_{Asc} - d_{East}\sin\delta_{Asc}\cos\alpha_{Asc} \\ &\quad - d_{North}\sin\delta_{Asc}\sin\alpha_{Asc} \\ d_{losDesc} &= d_{up}\cos\delta_{Desc} + d_{East}\sin\delta_{Desc}\cos\alpha_{Desc} \\ &\quad - d_{North}\sin\delta_{Desc}\sin\alpha_{Desc} \end{aligned} \tag{15}$$

which exploit the value of the off-nadir angle δ and the local heading angle α between the orbital ground track and the North direction. This latter can be found by computing the local slope of the ground track with (10) and then the complementary angle, which corresponds to the angle with respect to the North direction. The above-mentioned angles are visually represented in Figs. 5 and 6.

Figs. 16(a) and (b) show the projection along the LOS in correspondence to 1 cm deformation in the East-West or North-South directions, respectively, by setting an off-nadir angle of 30°. Moreover, for the sake of completeness, in this discussion Table VI reports the projected values in LOS for some Italian

cities at different latitudes. However, a consequence related to the near-horizontal slope of the Northernmost orbital passes is that in the Northern regions of the AoI we do not have orbits with different inclinations, as for the rest of Italy. In other words, since in the Northern areas the local heading angle tends to be 90° in both the ascending and descending cases, the system of equations (15) is simplified as follows:

$$\begin{aligned} d_{losAsc} &= d_{up}\cos\delta_{Asc} - d_{North}\sin\delta_{Asc} \\ d_{losDesc} &= d_{up}\cos\delta_{Desc} - d_{North}\sin\delta_{Desc} \end{aligned} \quad (16)$$

Assuming that both the ascending and descending passes work with the same beam ($\delta_{Asc} = \delta_{Desc}$), we obtain two linearly dependent equations that make it unfeasible to separate the Vertical deformation component (Up) from the planar one (North). Moreover, even if we entertain the assumption that the orbital passes operate in different beams, the values of $\cos\delta_{Asc}$ and $\sin\delta_{Asc}$ are so close to the corresponding descending values ($\cos\delta_{Desc}$ and $\sin\delta_{Desc}$) that the system in (16) results ill-conditioned in any case [45]. It would thus appear that this system is not capable, independently of the CSK/CSG exploitation, of resolving the Vertical and planar deformation components over these Northern regions of the AoI. However, it is also worth noting that, by launching the second NIMBUS batch with a different orbital inclination (say around 44°) in a left-looking acquisition mode, we can solve the problem of the system ill-conditioning.

To better understand this concept, without loss of generality, we may consider a scenario in which we have two MIO ascending passes in the North of the AoI, both using the same beam. One of these passes is in a right-looking mode while the other is in a left-looking mode. Hence, the observations will be made at off-nadir angles of δ_{right} e $-\ \delta_{left}$, respectively. Therefore, the system of equations becomes as follows:

$$\begin{aligned} d_{losAsc,right} &= d_{up}\cos\delta_{right} - d_{North}\sin\delta_{right} \\ d_{losAsc,left} &= d_{up}\cos\delta_{left} + d_{North}\sin\delta_{left} \end{aligned} \quad (17)$$

Thus, we have reduced the situation to a scenario in which the system is well-conditioned and the components d_{up} and d_{North} can be resolved [46].

TABLE VI
PROJECTION ALONG THE LOS OF 1 CM DEFORMATION IN N-S AND E-W DIRECTION FOR NIMBUS (MIO) AND CSK/CSG (SSO).

		NIMBUS (MIO)		**CSK/CSG (SSO)**	
City	**Latitude**	**N-S [cm]**	**E-W [cm]**	**N-S [cm]**	**E-W [cm]**
Bolzano	46°29'26"	0.480	0.140	0.122	0.485
Milan	45°27'51"	0.466	0.181	0.120	0.485
Bologna	44°29'38"	0.459	0.199	0.119	0.486
Florence	43°46'45"	0.454	0.210	0.118	0.486
Rome	41°53'30"	0.438	0.242	0.116	0.486
Naples	40°51'22"	0.428	0.258	0.115	0.487
Palermo	38°07'55"	0.412	0.283	0.113	0.487

A dedicated simulation activity on these issues is very relevant and, therefore, deserves future studies.

V. CONCLUSION AND FUTURE DEVELOPMENTS

This paper presented a constellation design focused on the X-band SAR sub-constellation NIMBUS of the IRIDE program. The primary goal is to discern which orbital configuration provides full coverage of the Italian territory, optimizing, at the same time, DInSAR performance in alignment with the ground motion community needs. In pursuing this result, a methodology, that considers preliminary system specifications and strict geometric constraints dictated by DInSAR, was discussed. The implemented tools turn out to be flexible to generate and manage Repeating Ground Track orbits of different nature (both MIO and SSO). In particular, it is proven that under the same 6 days of interferometric revisit time and equivalent SAR swath widths, the selected 49° MIO configuration with 6 satellites in a right-looking StripMap acquisition mode results in being highly effective in achieving satisfactory coverage of the overall Italian territory, with high spatial resolution. Subsequently, it has been demonstrated that the considered MIO scenario, in addition to providing valuable spatial coverage within a short DInSAR revisit time, does not significantly suffer from problems related to critical perpendicular baseline or geometric distortions that may limit the sub-constellation exploitation for DInSAR applications. Furthermore, in this MIO configuration, it is inferred that more than 40% of the North-South displacement component contributes to the LOS projection, in contrast to the low sensitivity of the SAR satellites operating in SSO with respect to this component. Thanks to this capability, it will be worthwhile to analyze, in the future, the synergy of the IRIDE NIMBUS MIO 6 satellites with other SSO X-band constellations working with similar spatial resolutions and wavelengths, such as the COSMO-SkyMed satellites of the first and second generation. Indeed, this may enable a detailed retrieval of the three-dimensional behavior of several displacement signals, introducing a cognitive component that has been missing so far.

Moreover, we remark that the quasi-horizontal behavior of the IRIDE NIMBUS orbital passes in the North of our AoI involves essentially two problems. The first concerns some foreshortening and layover effects in Northern Italy's Alps region that do not differ whether the orbital pass is ascending or descending. This implies that such areas will always be affected by these problems and, at least in this observing geometry, there is no way to improve their visibility. The second problem concerns the difficulty we still have in the Northern areas of Italy in solving the system to separate the Vertical and planar (North) deformation components if no additional SSO acquisitions are considered.

To address these issues, we propose, as future work, to optimize the orbital configuration of the second batch of 6 NIMBUS satellites, which is already planned to be launched after the first one. Indeed, as briefly shown, the refinement process is expected to enhance the overall constellation performance and to adjust some shortcomings of the first batch. For instance, we could think about arranging this second batch in an MIO as well, but in a left-looking observation geometry with an orbital

inclination angle of 44°, that could represent the first option to be considered. This will result in foreshortening/layover effects in the opposite mountain slopes with respect to the first batch, thus mitigating the overall impact of this effect, and will provide an independent equation to directly recover, from the NIMBUS SAR data, the North and Vertical deformation components. As already said, additional simulations and activities relevant to these issues are very relevant and, therefore, they are worth future analysis.

ACKNOWLEDGMENT

The digital elevation models of the analyzed areas were acquired through the NASA SRTM archive. The authors thank Dr. Andrea Taramelli and Dr. Serena Geraldini for their continuous support on the IRIDE program developments.

REFERENCES

[1] P. A. Rosen *et al.*, "Synthetic aperture radar interferometry," *Proc. IEEE*, vol. 88, no. 3, pp. 333–382, Mar. 2000.
[2] D. Massonnet, M. Rossi, C. Carmona, F. Adragna, G. Peltzer, K. Feigl, and T. Rabaute, "The displacement field of the Landers earthquake mapped by radar interferometry," *Nature*, vol. 364, no. 6433, pp. 138–142, Jul. 1993.
[3] G. Peltzer and P. A. Rosen, "Surface displacement of the 17 May 1993 Eureka Valley earthquake observed by SAR interferometry," *Science*, vol. 268, no. 5215, pp. 1333–1336, Jun. 1995.
[4] P. Lundgren, S. Usai, E. Sansosti, R. Lanari, M. Tesauro, G. Fornaro, and P. Berardino, "Modeling surface deformation observed with SAR interferometry at Campi Flegrei Caldera," *J. Geophys. Res.*, vol. 106, pp. 19 355–19 367, Sept. 2001.
[5] P. Berardino, G. Fornaro, R. Lanari, and E. Sansosti, "A new algorithm for surface deformation monitoring based on small baseline differential SAR interferograms," *IEEE Trans. Geosci. Remote Sens.*, vol. 40, no. 11, pp. 2375–2383, Nov. 2002.
[6] R. Lanari, O. Mora, M. Manunta, J. J. Mallorquì, P. Berardino, and E. Sansosti, "A small-baseline approach for investigating deformations on full-resolution differential SAR interferograms," *IEEE Trans. Geosci.Remote Sens.*, vol. 42, no. 7, pp. 1377–1386, Jul. 2004.
[7] O. Mora, J. J. Mallorquì, and A. Broquetas, "Linear and nonlinear terrain deformation maps from a reduced set of interferometric SAR images," *IEEE Trans. Geosci. Remote Sens.*, vol. 41, no. 10, pp. 2243–2253, Oct. 2003.
[8] M. Manunta, M. Marsella, G. Zeni, M. Sciotti, S. Atzori, and R. Lanari, "Two-scale surface deformation analysis using the SBAS-DInSAR technique: A case study of the city of Rome, Italy," *Int. J. Remote Sens.*, vol. 29, no. 6, pp. 1665–1684, 2008.
[9] M. Bonano, M. Manunta, M. Marsella, and R. Lanari, "Long-term ERS/ENVISAT deformation time-series generation at full spatial resolution via the extended SBAS technique," *Int. J. Remote Sens.*, vol. 33, pp. 4756–4783, Aug. 2012.
[10] A. Ferretti, C. Prati, and F. Rocca, "Nonlinear subsidence rate estimation using permanent scatterers in differential SAR interferometry," *IEEE Trans. Geosci. Remote Sens.*, vol. 38, no. 5, pp. 2202–2212, Sep. 2000.
[11] A. Ferretti, C. Prati, and F. Rocca, "Permanent scatterers in SAR interferometry," *IEEE Trans. Geosci. Remote Sens.*, vol. 39, no. 1, pp. 8–20, Jan. 2001.
[12] C. Werner, U. Wegmüller, T. Strozzi, and A. Wiesmann, "Interferometric point target analysis for deformation mapping," in *Proc. IEEE IGARSS*, Toulouse, France, Jul. 21–25, 2003, vol. 7, pp. 4362–4364.
[13] M. Bonano, M. Manunta, A. Pepe, L. Paglia and R. Lanari, "From previous C-band to new X-band SAR systems: Assessment of the DInSAR mapping improvement for deformation time-series retrieval in urban areas", *IEEE Trans. Geosci. Remote Sens.*, vol. 51, no. 4, pp. 1973-1984, Apr. 2013.
[14] L. Yu, T.L. Yang, Q. Zhao, M. Liu and A. Pepe, "The 2015–2016 ground displacements of the Shanghai coastal area inferred from a combined COSMO-SkyMed/Sentinel-l DInSAR analysis", *Remote Sens.*, vol. 9, no. 11, pp. 1-19, Nov. 2017.
[15] S.L. Ullo, P. Addabbo, D. Di Martire, S. Sica, N. Fiscante, L. Cicala, C.V. Angelino, "Application of DInSAR technique to high coherence Sentinel-1 images for dam monitoring and result validation through in situ measurements", *IEEE J. Sel. Topics Appl. Earth Observ. Remote Sens.*, vol. 12, no. 3, pp. 875-890, Mar. 2019.
[16] M. Manunta, C. De Luca, I. Zinno, F. Casu, M. Manzo, M. Bonano, R. Lanari, "The parallel SBAS approach for Sentinel-1 interferometric wide swath deformation time-series generation: Algorithm description and products quality assessment", *IEEE Trans. Geosci. Remote Sens.*, vol. 57, no. 9, pp. 6259-6281, May 2019.
[17] K. Pawluszek-Filipiak, K., A. Borkowski, "Integration of DInSAR and SBAS techniques to determine mining-related deformations using sentinel-1 data: The case study of Rydułtowy mine in Poland", *Remote Sens.*, vol. 12, 2020.
[18] Y. Roa, P. Rosell, A. Solarte, L. Euillades, F. Carballo, S. García, et al., "First assessment of the interferometric capabilities of SAOCOM-1A: New results over the Domuyo Volcano Neuquén Argentina", *Journal of South American Earth Sciences*, vol. 106, pp. 102882, 2021.
[19] A. Ng, L. Ge, Z. Du, S. Wang and C. Ma, "Satellite radar interferometry for monitoring subsidence induced by longwall mining activity using Radarsat-2 Sentinel-1 and ALOS-2 data", *Int. J. Appl. Earth Observ. Geoinf.*, vol. 61, pp. 92-103, Sept. 2017.
[20] V. Ignatenko, P. Laurila, A. Radius, L. Lamentowski, O. Antropov and D. Muff, "ICEYE microsatellite SAR constellation status update: Evaluation of first commercial imaging modes", *Proc. IEEE Int. Geosci. Remote Sens. Symp.*, pp. 3581-3584, Sep. 2020.
[21] D. Castelletti, G. Farquharson, C. Stringham, M. Duersch and D. Eddy, "Capella space first operational SAR satellite", *Proc. IEEE Int. Geosci. Remote Sens. Symp.*, pp. 1483-1486, 2021.
[22] Y. Ulybyshev, "A general analysis method for discontinuous coverage satellite constellations", *J. Guid. Control Dyn.*, vol. 38, no. 12, pp. 2475-2482, Aug. 2015.
[23] Y. N. Razoumny, "Fundamentals of the route theory for satellite constellation design for Earth discontinuous coverage. Part 1: Analytic emulation of the Earth coverage", *Acta Astronaut*, vol. 128, pp. 722-740, 2016.
[24] N. H. Crisp, S. Livadiotti and P. C. E. Roberts, A Semi-Analytical Method for Calculating Revisit Time for Satellite Constellations with Discontinuous Coverage, Jul. 2019, [online] Available: http://arxiv.org/pdf/1807.02021v1.
[25] O. Abdelkhalik and A. Gad, "Optimization of space orbits design for earth orbiting missions", *Acta Astronautica*, vol. 68, no. 7–8, pp. 1307-1317, 2011.
[26] X. Dong, Y. Sui, Y. Li, Z. Chen, and C. Hu, "Repeat Ground Track SAR Constellation Design Using Revisit Time Image Extrapolation and Lookup-Table-Based Optimization," *IEEE Trans. Geosci.Remote Sens.*, vol. 61, pp. 1-13, 2023.
[27] D. Casanova, M. Avendaño and D. Mortari, "Seeking GDOP-optimal flower constellations for global coverage problems through evolutionary algorithms", *Aerosp. Sci. Technol.*, vol. 39, pp. 331-337, 2014.
[28] H. W. Lee, S. Shimizu, S. Yoshikawa and K. Ho, "Satellite constellation pattern optimization for complex regional coverage", *J. Spacecraft Rockets*, vol. 57, no. 6, pp. 1309-1327, Nov. 2020.
[29] Z. Song, G. Dai, M. Wang and X. Chen, "A novel grid point approach for efficiently solving the constellation-to-ground regional coverage problem", *IEEE Access*, vol. 6, pp. 44445-44458, Aug. 2018.
[30] F. Casu and A. Manconi, "Four-dimensional surface evolution of active rifting from spaceborne SAR data", *Geosphere*, vol. 12, no. 3, pp. 697-705, 2016.
[31] M. Manzo, G.P. Ricciardi, F. Casu, G. Ventura, G. Zeni, S. Borgström, P. Berardino, C. Del Gaudio, R. Lanari, "Surface deformation analysis in the Ischia Island (Italy) based on spaceborne radar interferometry", *Journal of Volcanology and Geothermal Research*, vol. 151, no. 4, pp.399-416, 2006.
[32] F. Greene Gondi, J. Eppler, and R. Caves, "Enabling 3D Deformation Monitoring with the CHORUS SAR Constellation," in *FRINGE*, Leeds, England, 2023.
[33] The European Space Agency, Apr. 2023, IRIDE: La squadra è al completo, [online] Available: https://www.esa.int/Space_in_Member_States/Italy/IRIDE_La_squadra_e_al_completo.
[34] D-Orbit, A SATELLITE CONSTELLATION FOR THE ITALIAN PUBLIC ADMINISTRATION, [online] Available: https://www.dorbit.space/iride-nox.
[35] Thales Alenia Space, Mar.2023, Italy's new constellation of innovative and flexible Earth observation satellites to monitor Italy and Europe, [online] Available: https://www.thalesaleniaspace.com/en/press-releases/thales-alenia-space-wins-contracts-iride-radar-and-optical-satellites.
[36] M. Capderou, Handbook of Satellite Orbits: From Kepler to GPS, Berlin, Germany:Springer, 2014.

[37] D. A. Vallado, Fundamentals of Astrodynamics and Applications, Berlin, Germany:Springer, 2001.
[38] J. Wertz, Mission Geometry: Orbit and Constellation Design and Management: Spacecraft Orbit and Attitude Systems, Portland, OR, USA:Microcosm Press, 2001.
[39] C. Wagner, "A prograde geosat exact repeat mission?", *Journal of the Astronautical Sciences,* vol. 39, pp. 313-326,1991.
[40] TAITUS SOFTWARE, SaVoir, [online] Available: https://taitussoftware.com/products/applications/savoir.
[41] G. Franceschetti and R. Lanari, Synthetic Aperture Radar Processing. Boca Raton, FL, USA: CRC Press, 1999.
[42] D. Notti, J. C. Davalillo, G. Herrera and O. Mora, "Assessment of the performance of X-band satellite radar data for landslide mapping and monitoring: Upper Tena Valley case study", *Natural Hazards Earth System Sci.*, vol. 10, no. 9, pp. 1865-1875, 2010.
[43] ASI, ITALIAN SPACE AGENCY UPGRADES ACCESS TO MAPITALY DATA, [online] Available: https://www.asi.it/en/2023/12/asi-italian-space-agency-upgrades-access-to-mapitaly-data.
[44] C. De Luca, I. Zinno, M. Manunta, R. Lanari, and F. Casu, “Large areas surface deformation analysis through a cloud computing P-SBAS approach for massive processing of DInSAR time series,” Remote Sens. Environ., vol. 202, pp. 3–17, Dec. 2017.
[45] G. Strang, Linear Algebra and Its Applications. Orlando, FL: Harcourt Brace Jovanovich, 1988.
[46] F. Guzzetti, M. Manunta, F. Ardizzone, A. Pepe, M. Cardinali, G. Zeni, R. Lanari, "Analysis of ground deformation detected using the SBAS-DInSAR technique in Umbria central Italy", *Pure Appl. Geophys.*, vol. 166, no. 8, pp. 1425-1459, 2009.